IEEE Photonics Journal
An IEEE Photonics Society Publication

Open Access

Transmission of Infrared Radiation Through Metallic Photonic Crystal Structures

Volume 5, Number 5, October 2013

Reyhaneh Soltanmoradi
Qin Wang
Min Qiu
Jan Y. Andersson

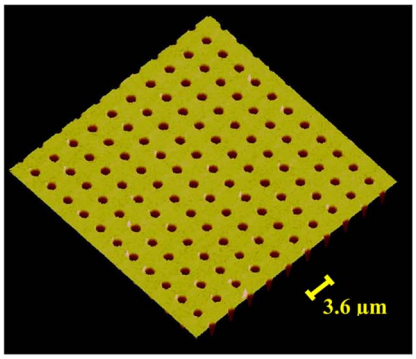

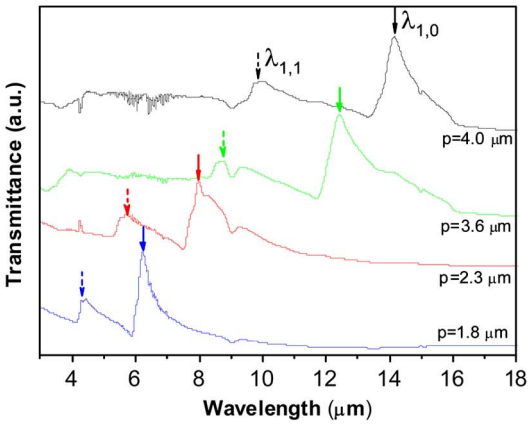

DOI: 10.1109/JPHOT.2013.2278527
1943-0655 © 2013 IEEE

IEEE photonics SOCIETY

IEEE

Transmission of Infrared Radiation Through Metallic Photonic Crystal Structures

Reyhaneh Soltanmoradi,[1] Qin Wang,[2] Min Qiu,[1] and Jan Y. Andersson[2]

[1]School of Information and Communication Technology, Royal Institute of Technology (KTH), 164 40 Kista, Sweden
[2]Department of Nanoelectronics, Acreo Swedish ICT AB, 164 40 Kista, Sweden

DOI: 10.1109/JPHOT.2013.2278527

Manuscript received June 16, 2013; revised August 4, 2013; accepted August 7, 2013. Date of publication August 15, 2013; date of current version September 30, 2013. This work was supported by the industry excellence center IMAGIC based at Acreo Swedish ICT AB financed by the Swedish Governmental Agency for Innovation Systems (Vinnova), the Knowledge Foundation, and several industry partners. The Swedish Foundation for Strategic Research (SSF) and Vetenskapsrådet (VR) foundation provided additional project support. Corresponding author: Q. Wang (e-mail: qin.wang@acreo.se).

Abstract: Monolithic integration of a metallic photonic crystal (mPhC) structure onto semiconductor infrared (IR) photodetectors can enhance the detector performances. In order to experimentally investigate the parameters involved in optimizing the transmission spectra of the mPhC structures matching the detector operating wavelength in mid- and long-wave IR (MWIR and LWIR) regimes, square thin gold (Au) hole arrays having periodicities of 4.0, 3.6, 2.4, and 1.8 μm with various fill factors were fabricated on Si or GaAs substrates in a wafer scale. The thicknesses of the Au films are 50, 100, and 200 nm, respectively. Through this systemic study, suitable mPhC structures were revealed that can be readily integrated onto our type-II InGaSb-based quantum dot MWIR and LWIR photodetectors.

Index Terms: Infrared photodetectors, plasmonics, subwavelength structures, metallic photonic crystal.

1. Introduction

Infrared (IR) imaging and sensing have many applications in security, night vision, surveillance, search and rescue, industrial process control and medical diagnosis. These applications have driven their related component/system's markets to grow rapidly [1]. Nowadays, quantum well infrared photodetectors (QWIP), small-bandgap bulk alloy HgCdTe (MCT) and InSb IR detectors are used for state-of-the-art IR cameras, however, IR detectors with better performance and low cost are desired for development of next generation IR camera systems. Various solutions and alternatives to realize such goals have been widely explored, for instance, intra-subband transition based type-I quantum dot infrared photodetectors (QDIPs) [2]–[4] and type-II strained layer superlattices (T2SLs) IR detectors [5]–[7]. Recently, type-II In(Ga)Sb quantum dot (QD) IR detectors with high operating temperatures up to 225 K have been reported as a means of detection mechanism based on inter-band transitions from bound hole states in the QDs to continue states in the surrounding bulk material [8], [9], so-called dot-to-bulk (D2B) detectors, as detailed in our previous publication [9].

Apart from above-mentioned new type quantum structures based on a bottom up approach, recently the promotion of top-down approach to enhance the IR detector's response and functionality has been initiated by manipulating the incident IR radiation [10]–[12]. The approach is to integrate well-designed metallic periodic subwavelength hole arrays, so-called metallic photonic crystal (mPhC), onto the IR detectors. Progress in this research filed is going very fast, monolithically

integrated plasmonic IR QD camera and multicolor IR thermal detection have been achieved [13], [14] very recently, and related theoretic modeling is continually active to pave the way to novel design strategies [15]–[17].

When an electromagnetic wave impinges on a metallic surface, there is an interaction between the photons and the metal's free electrons. At a certain beam angle the surface plasmon resonance (SPR) can be induced and the incident photons are spatially localized at the interface between the metal and beneath dielectric material, which results in an electromagnetic surface plasmon wave (SPW). It should be noted that the signs of the dielectric constant of the two media forming the interface must be opposite in order to trap the photons at the interface. Several metals, such as gold (Au), silver (Ag), platinum (Pt), copper (Cu), chromium (Cr) and titanium (Ti), are known to be applicable to form the SPW when depositing them on the top of semiconductor materials.

The SPW formed at the metal/semiconductor interface upon IR radiation has a typical decay length of several microns, and its resonance wavelength is determined by the mPhC's lattice constant [15]. In our previous simulation work [10], the photocurrent enhancement of the mPhC integrated QDIP was predicted by numerically calculating both the optical transmission and diffraction through the mPhC and the light-matter interaction in the QDs within a propagation length shorter than the SPW's decay length. Apparently, having the interaction of this SPW with the IR detector active material is more efficient than the incident photons just passing through the detector by a single path. Therefore, the absorption and responsivity of the IR detectors can be improved in accordance with the designed strength of the SPW evanescent field [15], [16].

In this paper, a series of the subwavelength square hole arrays with periodicities 4 μm, 3.6 μm, 2.4 μm and 1.8 μm and a range of fill factors were fabricated in Au layers with thicknesses of 50 nm, 100 nm and 200 nm on top of 4″ Si or GaAs substrates, respectively. This study is aiming to optimize mPhC structures, and thereby providing an effective integration solution for enhancing performance of our D2B IR detectors. The D2B IR detector has promising potential to operate at high temperatures in the MWIR/LWIR regimes, but its response was limited by numbers of the D2B repeats in the active region of the detectors [9]. We experimentally demonstrated that adjusting the mPhC structure parameters such as the lattice constant can tune the SPR to match the IR detector's operating wavelength. In particular, the wafer-scale mPhC fabrication enables direct adopt optimized structures into the IR detector processing line.

It is believed that integration of the mPhC structures onto IR detectors is not only a way to enhance their responsivity owing to the coupling of SPW with the IR absorber, but also to offer advantageous for hyper-spectral imaging due to the mPhC providing a surface with frequency selectivity capacity. The experimentally systemic study of the mPhC structures in this work may also help to provide in understanding and designing complex periodic or aperiodic metallic structures in applying plasmonic structures to sensors, photovoltaics, light-emitting diodes and lasers.

2. Fabrication and Structural Characterization of mPhC

The mPhC structures with different Au thicknesses and varied hole diameters/pitches were fabricated on double-side polished 4-in Si or GaAs substrates. The process was started by depositing a thin Ti film as adhesive layer followed by an Au film with varied thicknesses of 50 nm, 100 nm and 200 nm, respectively. The designed mPhC structures were patterned using an XLS 7500/2145 i-line stepper with a magnification of 1/5. The structures were then etched into the Au film by wet etching. It is worth to note that this is a wafer-scale fabrication method enabling direct adaption of the mPhC fabrication step into current online IR detector product processing.

The array with pitch sizes of 4.0 μm, 3.6 μm, 2.3 μm, and 1.8 μm were obtained according to the designs, with hole diameters being controlled by their etching time from an initial diameter of 1 μm. Fig. 1 shows examples of the arrays having the same pitch of 3.6 μm but with different hole diameter of 1.6 μm, 2.1 μm, 2.8 μm, and 3.1 μm controlled by wet etching time of 5, 10, 20, and 30 seconds (s), respectively. The corresponding fill factors are 41%, 50%, 73%, and 84%, as defined by the non-metal covered area divided by the total area of the mPhC structures. The diameter of the holes increases with etching time due to lateral etching effect caused by the well established selective Au wet etching.

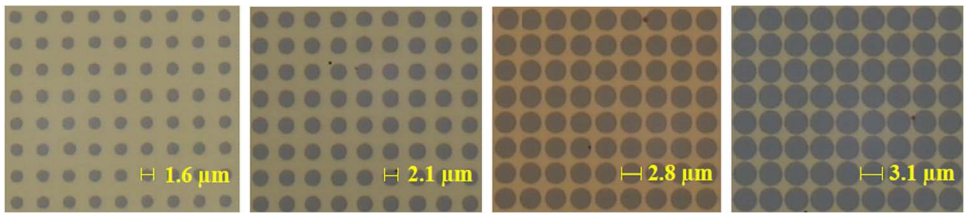

Fig. 1. Microscope images of the mPhC structures with different hole diameters controlled by etching time of 5, 10, 20, and 30s, respectively.

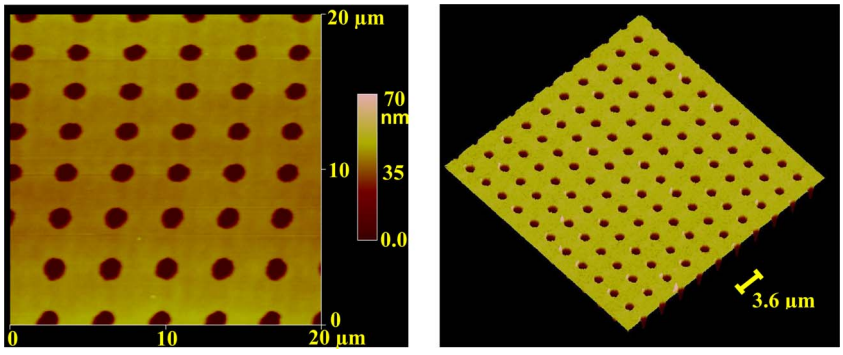

Fig. 2. Top-view (left) and 3D (right) AFM images of the square holes array with a pitch of 3.6 μm and 1.6 μm in diameter.

The tomography, etching depth of the holes were characterized by atomic force microscopy (AFM) and scanning electron microscopy (SEM) measurements. Fig. 2 shows the top-view (left) and 3D AFM (right) images of a 50 nm thick mPhC structure etched for 5 s, with an original hole diameter in the photo resist layer of 1 μm. AFM analysis revealed that the hole depth is in agreement with the deposited Au film thickness, which was confirmed by cross section SEM measurement results.

The transmittance spectra of the mPhC structures were measured using a Bruker Vertex 70V Fourier transform infrared (FTIR) spectrometer. The spectra were recorded using air as background in the air ambient. The samples were perpendicularly illuminated by a non-polarized IR light source, and the transmitted light was then collected by an MCT liquid nitrogen-cooled detector. The typical spectral resolution of 4 cm^{-1} was used, but higher spectral resolutions were also explored for some selected samples.

3. Results and Discussions

The transmittance spectra of all fabricated mPhC structures were measured and categorized into four groups for comparison, which are detailed in the following sub-sections.

3.1. Modification of SPR by the mPhC Pitch

Fig. 3 shows the transmittance spectra of the mPhC structures on Si substrate with a pitch of 4.0 μm, 3.6 μm, 2.3 μm, and 1.8 μm, respectively, hole depth of 100 nm determined by the Au layer thickness and fill factor of 73%. To manage the samples having the same non-metal covered area, a series of filters were carefully designed and used in front of the mPhC samples facing the incident IR radiation. In this way, the intensity of the different transmission data can be compared directly.

SPR wavelength can be calculated from equation (1), where *i* and *j* represent the orders of the plasmonic modes in the *x*- and *y*-directions in the 2D orthogonal spatial coordination, p is the pitch,

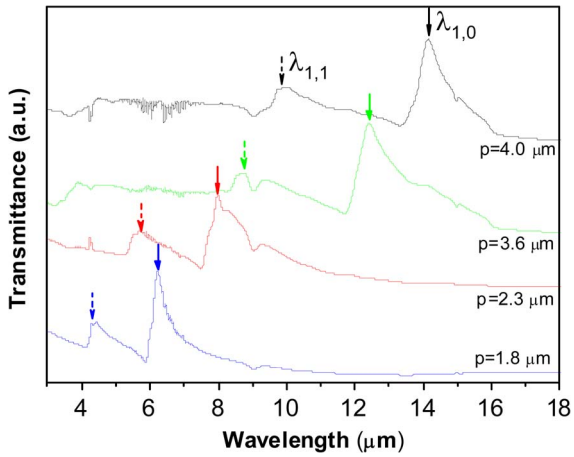

Fig. 3. Transmittance spectra of mPhC structures on Si substrate with varied periodicity. An offset of each spectrum was introduced for clarification, whereas their respective amplitudes remained unchanged without modification. Solid and dash-line arrows in the figure represent $\lambda_{1,0}$ and $\lambda_{1,1}$, respectively.

TABLE 1

Summary of experiment and calculated SPR wavelengths at designed pitch

	Experiment $\lambda_{i,j}$ (μm)		Calculated $\lambda_{i,j}$ (μm)	
Pitch (μm)	*i=1 j=0*	*i=1 j=1*	*i=1 j=0*	*i=1 j=1*
4.0	14.2	9.8	13.8	9.8
3.6	12.4	8.7	12.4	8.8
2.3	8.0	5.6	7.9	5.6
1.8	6.2	4.4	6.2	4.4

ε_m and ε_d are dielectric constants of the metal and the semiconductor

$$\lambda_{ij} = \frac{p}{\sqrt{i^2 + j^2}} Re\left\{ \left[\frac{\varepsilon_m \varepsilon_d}{\varepsilon_m + \varepsilon_d} \right]^{1/2} \right\}. \quad (1)$$

Table 1 shows that both the first harmonic (fundamental mode) and the second harmonic SPR peak wavelengths of the mPhC structures in Fig. 3 occur in good agreement with their corresponding theoretic predicted wavelengths described by the equation (1). In the calculation, the dielectric constants of GaAs and Si in the LWIR region are 10.9 and 11.9, whereas the negative dielectric constant of Au varies with wavelength, its real part is much larger than that of Si or GaAs. For example ε_m is $-3206.7 + i1569.4$ at 10.2 μm [13] is used in this work.

The consistency of the experimental and calculated SPR wavelengths indicates a very well controlled mPhC fabrication process in this work. It also provides valuable information for designing corresponding mPhC structures to accurately match the desired operating wavelengths of the IR detectors.

3.2. Effect of the mPhC Fill Factor on IR Transmittance

Fig. 4(a) and (b) show the transmittance spectra of the mPhC structures with varying hole diameters at the fixed pitch of 3.6 μm and 4.0 μm on Si and GaAs substrate, respectively. The depth of the holes is 100 nm, and the hole diameter was readily controlled by wet etching time, some examples are illustrated in Fig. 1.

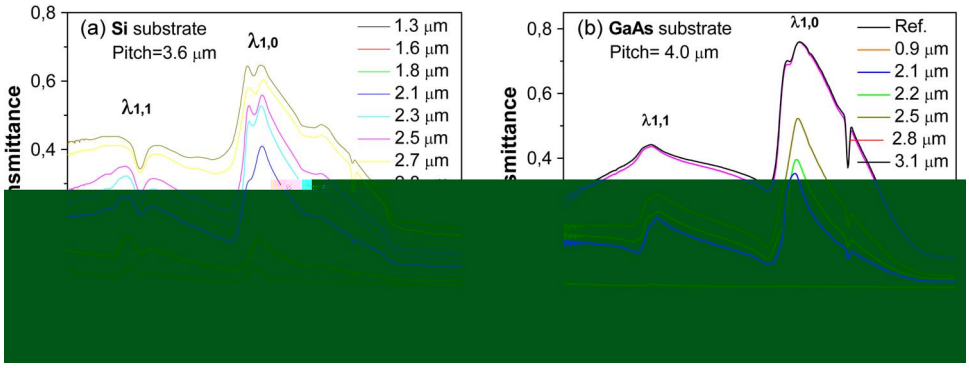

Fig. 4. Transmittance spectra of mPhC structures on Si and GaAs substrates with different hole diameters at fixed periodicities of 3.6 μm and 4 μm, respectively.

Longer etching times formed larger holes, which caused a larger fill factor. The transmittance spectra shown in Fig. 4(a) and (b) reveal that their SPR peaks are located at the same wavelengths although the hole diameter increased owing to longer etching time, whereas the intensity of the transmittance increased in corresponding higher fill factor cases. However, the SPR becomes less confined and the bandwidth wider with increasing hole diameter. Apparently, the hole diameters of 1.3 μm and 0.9 μm of the mPhC samples on Si and GaAs, respectively, gave too low transmittance to obtain clear SPR features. These results indicate that a trade-off must be considered between transmission intensity and wavelength selectivity when designing the mPhC structures. The good trade-off will be helpful to get a reasonable intensity of transmittance signal that eventually arrives at the IR detection absorber located beneath the mPhC structure, and still keep a good SPR confinement.

It is worth to note that a transmittance spectrum of a sample coated with 100 nm Au without mPhC marked as Ref. in Fig. 4(b) had very low transmittance and did not show any SPR peaks as other mPhC structures had.

3.3. Modification of SPR by the Hole Depth

An optimum hole depth can provide the conditions of the best possible selectivity of the transmission peak and the most favorable amplitude. Fig. 5(a)–(d) illustrate the transmittance spectra from the mPhC samples on Si substrate with two hole depths of 100 nm and 200 nm and a pitch of 3.6 μm at hole diameters of 2.7 μm, 2.5 μm, 2.0 μm, and 1.6 μm, respectively. The results demonstrate that the thicker the metal layers the lower the transmission would be for hole diameters larger than 2 μm. This can be explained by the fact that deeper holes result in a narrower bandwidth of the transmission peak, which can enhance the selectivity and Q factor that ensures a lower rate of energy loss. For hole diameters less than 2 μm, however, the opposite is true and the transmitted intensity increases with increasing layer thickness as seen in Fig. 5(d). This might be caused by a better in-plane optical confinement with very small hole diameters, which reduces scattering losses at the mode energy [16].

3.4. Impact of the Substrate on the SPR

According to equation (1), the dielectric constant of the material beneath the mPhC also plays an important role for the location of the SPR wavelength. To verify this effect, transmittance spectra of the mPhC on Si and GaAs substrates with Au layer thickness of 100 nm and array pitch of 4 μm were compared as shown in Fig. 6(a) and (b). The difference in (a) and (b) is the hole diameter of the mPhC structures, 2.2 μm (a) and 2.4 μm (b).

GaAs is transparent for IR radiation in MWIR and LWIR regimes, and it is commonly used as IR detector base material such as QWIP and QDIP. Its dielectric constant is 10.9 as mentioned above, which is smaller than that of Si (11.9). The blue shift that observed in comparison with the SPR peak of Si-based mPhC structures is likely to be caused by this difference of dielectric constant. This study provided a clear guidance for designing effective mPhC structures with consideration of their

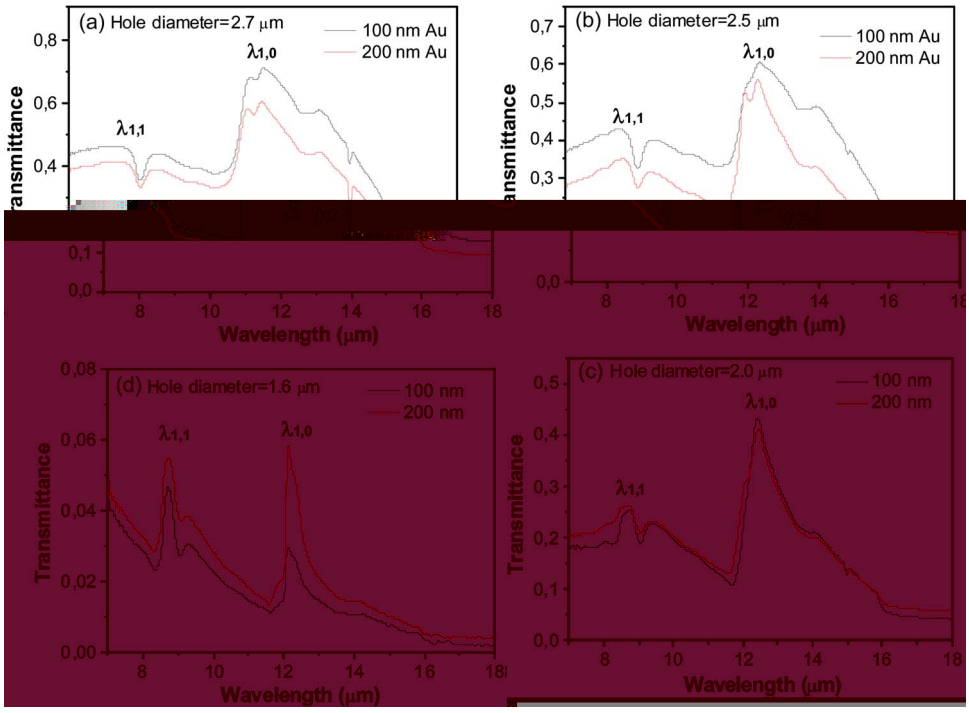

Fig. 5. Transmittance spectra of mPhC structures on Si substrate with different hole depths and diameters at fixed periodicity of 3.6 μm.

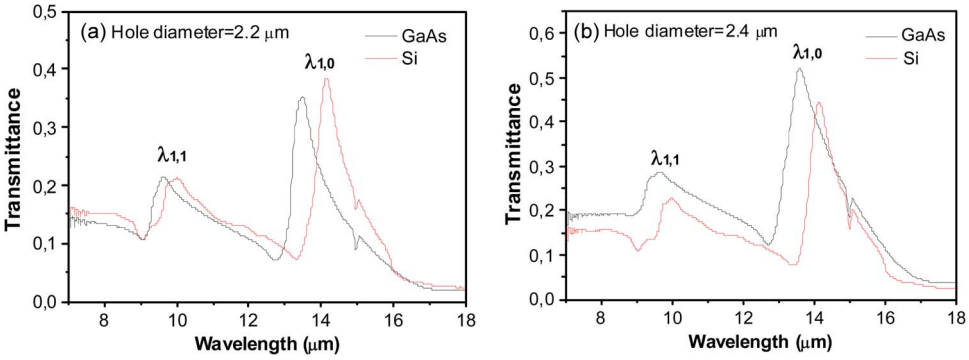

Fig. 6. Comparison of transmittance spectra of mPhC structures on GaAs and Si substrate with 4 μm pitch at two hole diameters of 2.2 μm (a) and 2.4 μm (b).

beneath materials. For example dielectric constant of InAs is needed to count for designing the mPhC structures for our D2B IR detectors, where InAs is main bulk material to embed the InGaSb type-II QDs.

4. Prediction of Performance Enhancement of D2B IR Detectors by Integration of mPhC

As described above the D2B detectors demonstrated possibility of higher operating temperatures, which is promising for significantly reducing the IR camera's cost [9], [10]. However, its responsivity is still low due to limited QD stack numbers govern by the material lattice mismatch and epitaxy growth time. The photoresponse and quantum efficiency of the D2B detectors can be expected to be improved by integrating the mPhC structure onto the devices. The improvement can be attributed to coupling of the SPW with the quantum dots as schematically illustrated in Fig. 7(a),

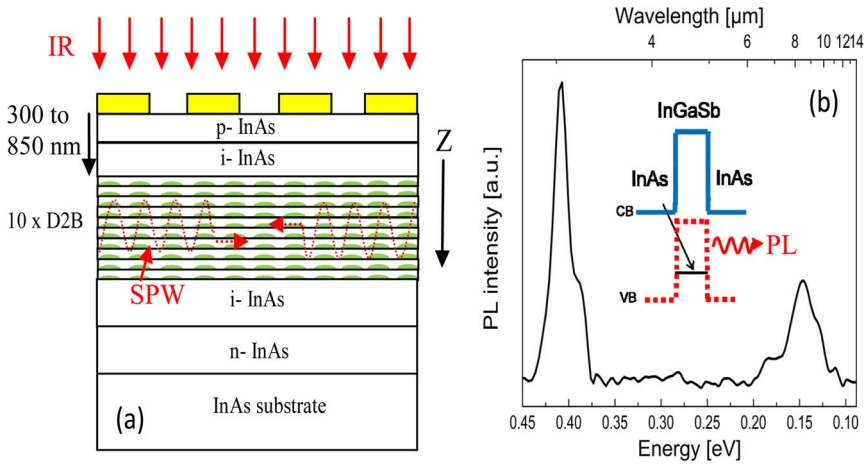

Fig. 7. (a) Schematic illustration (not in scale) of SPW coupling with the type-II InGaSb QDs caused by mPhC integration under IR irradiation. (b) PL measured at 77 K from a single layer $In_{0.5}Ga_{0.5}Sb$ QD sample, its band diagram and interband transitions schematically shown in the insert.

which helps IR absorption more efficiently in comparison with the IR incident wave just passing through the QDs by a single optical path. The InGaSb QDs is located from 300 nm to 850 nm from the device surface corresponding to different device designs that reported in our former paper [9]. The total thickness of 10 repeats of the D2B is about 850 nm, their locations along the Z-direction as marked in Fig. 7(a) are well confined within the SPW decay length [14]. The surface-plasmon damping coefficient (α) along the Z-direction can be approximated by equation (2) [16]

$$\alpha \approx 4\pi n_m n_d^3/(\lambda k_m^3) \tag{2}$$

where k_m is the imaginary part of the metal's refractive index, and n_m (n_d) is the real part of the metal (semiconductor) index of refraction, and λ is the wavelength. The $1/(\lambda k_m^3)$ dependence of the propagation loss shows that the SPW loss becomes very small at long wavelengths.

Fig. 7(b) shows photoluminescence (PL) of a single layer $In_{0.5}Ga_{0.5}$ Sb D2B structure, and the peaks observed at 3.1 μm and 8.5 μm are attributed to the InAs matrix material and QD-related type-II interband transitions as shown in the insert of Fig. 7(b) [9]. Notably, the transmittance spectrum of the mPhC structure with pitch of 2.3 μm as shown in Fig. 3 has an SPR $\lambda_{1,0}$ at about 8 μm, which approximately matches the PL peak of the D2B structure shown in Fig. 7(b). To integrate the mPhC on the top of individual D2B detectors, a fine tuning the pitch of the mPhC and also considering the dielectric constant of InAs are needed. This mPhC integration work will be carried out in a near future as a follow-up of the current work.

In addition, the mPhC structure can be used as part of the detector's top contact, which can help to improve the electric field distribution across the pin diode-type detectors. In fact, the fabrication of such mPhCs is very well compatible even with a focal plane array (FPA) process [11].

5. Conclusion

In summary, we demonstrate SPR from a series of Au-based mPhC structures that were processed in wafer-scale on Si or GaAs substrates, which can be readily integrated onto single pixel MWIR/LWIR photodetectors and their FPAs. This integration approach is promising to enhance detector's responsivity owing to coupling of SPW to detection active materials such as QDs at specific designed operating wavelengths. In particular, the wafer-scale mPhC fabrication is very well compatible with current IR photodetector product processing lines, which is not only greatly beyond a mere lab-based proof of concept but enables possibility of cost-effective high-performance IR photodetector products.

Acknowledgment

The authors would like to thank Dr. I. Petermann from Acreo Swedish ICT AB for valuable discussions.

References

[1] A. Rogalski, "Material considerations for third generation infrared photon detectors," *Infrared Phys. Technol.*, vol. 50, no. 2/3, pp. 240–252, Apr. 2007.
[2] D. Z. Ting, S. V. Bandara, S. D. Gunapala, J. M. Mumolo, S. A. Keo, C. J. Hill, J. K. Liu, E. R. Blazejewski, S. B. Rafol, and Y. C. Chang, "Submonolayer quantum dot infrared photodetector," *Appl. Phys. Lett.*, vol. 9, no. 11, pp. 111107-1–111107-3, Mar. 2009.
[3] M. Razeghi, W. Zhang, H.-C. Lim, S. Tsao, J. Szafraniec, M. Taguchi, and B. Movaghar, "Focal plane arrays based on quantum dot infrared photodetectors," in *Proc. SPIE*, 2005, vol. 5838, pp. 125–136.
[4] L. Hoglund, C. Asplund, Q. Wang, S. Almqvist, H. Malm, E. Petrini, J. Y. Andersson, and P. O. Holtz, "Origin of photocurrent in lateral quantum dots-in-a-well infrared photodetectors," *Appl. Phys. Lett.*, vol. 88, no. 21, pp. 213510-1–213510-3, May 2006.
[5] C. J. Hill, J. V. Li, J. M. Mumolo, and S. D. Gunapala, "MBE grown type-II MWIR and LWIR superlattice photodiodes," *Infrared Phys. Technol.*, vol. 50, no. 2/3, pp. 187–190, May 2007.
[6] S. Bogdanov, B. Nguyen, A. M. Hoang, and M. Razeghi, "Surface leakage current reduction in long wavelength infrared type-II InAs/GaSb superlattice photodiodes," *Appl. Phys. Lett.*, vol. 98, no. 18, pp. 183501-1–183501-3, May 2011.
[7] N. Gautam, H. S. Kim, S. Myers, E. Plis, M. N. Kutty, M. Naydenkov, B. Klein, L. R. Dawson, and S. Krishna, "Heterojunction bandgap engineered photodetector based on type-II InAs/GaSb superlattice for single color and bicolor infrared detection," *Infrared Phys. Technol.*, vol. 54, no. 3, pp. 273–277, May 2011.
[8] C. J. Hill, A. Soibel, S. A. Keo, J. M. Mumolo, D. Z. Ting, and S. D. Gunapala, "Mid-infrared quantum dot barrier photodetectors with extended cutoff wavelengths," *Electron. Lett.*, vol. 46, no. 18, pp. 1286–1287, Sep. 2010.
[9] O. Gustafsson, A. Karim, J. Berggren, Q. Wang, C. Reuterskiöld-Hedlund, C. Ernerheim-Jokumsen, M. Soldemo, J. Weissenrieder, S. Persson, S. Almqvist, U. Ekenberg, B. Noharet, C. Asplund, M. Göthelid, and J. Y. Andersson, "Photoluminescence and photoresponse from InSb/InAs-based quantum dot structures," *Opt. Exp.*, vol. 20, no. 19, pp. 21 264–21 271, Sep. 2012.
[10] S. Hellström, Z. H. Chen, Y. Fu, M. Qiu, R. Soltanmoradi, Q. Wang, and J. Y. Andersson, "Increased photocurrent in quantum dot infrared photodetector by subwavelength hole array in metal thin film," *Appl. Phys. Lett.*, vol. 96, no. 11, pp. 231110-1–231110-3, Jun. 2010.
[11] S. C. Lee, S. Krishna, and S. R. J. Brueck, "Plasmonic-enhanced photodetectors for focal plane arrays," *IEEE Photon. Technol. Lett.*, vol. 23, no. 14, pp. 935–937, Jul. 2011.
[12] P. Vasinajindakaw, J. Vaillancourt, G. Gu, and X. J. Lu, "Surface plasmonic enhanced polarimetric longwave infrared photodetection with band pass spectral filtering," *Semicond. Sci. Technol.*, vol. 27, no. 6, p. 065005, Jun. 2012.
[13] S. J. Lee, Z. Ku, A. Barve, J. Montoya, W. Y. Jang, S. R. J. Brueck, M. Sundaram, A. Reisinger, S. Krishna, and S. K. Noh, "A monolithically integrated plasmonic infrared quantum dot camera," *Nat. Commun.*, vol. 2, no. 4, p. 286, Apr. 2011.
[14] F. L. Mao, J. J. Xie, S. Y. Xiao, S. Komiyama, W. Lu, L. Zhou, and H. An, "Plasmonic light harvesting for multicolor infrared thermal detection," *Opt. Exp.*, vol. 14, no. 1, p. 295, Jan. 2013.
[15] C. Genet and T. W. Ebbesen, "Light in tiny holes," *Nature*, vol. 445, no. 7123, pp. 39–46, Jan. 2007.
[16] M. Bahriz, V. Moreau, R. Colombelli, O. Crisafulli, and O. Painter, "Design of mid-IR and THz quantum cascade laser cavities with complete TM photonic bandgap," *Opt. Exp.*, vol. 15, no. 10, pp. 5948–5965, May 2007.
[17] F. V. Beijnum, C. Retif, C. B. Smiet, H. Liu, P. Lalanne, and M. P. v.Exter, "Quasi-cylindrical wave contribution in experiments on extraordinary optical transmission," *Nature*, vol. 492, no. 20, pp. 411–414, Dec. 2012.